Postselection-free, hyperentangled photon pairs in a periodically poled lithium-niobate ridge waveguide

Ramesh Kumar, Vikash Kumar Yadav, and Joyee Ghosh*
Department of Physics, Indian Institute of Technology Delhi, New Delhi 110016, India

(Received 31 May 2020; accepted 8 September 2020; published 25 September 2020)

In this paper, we propose the generation of hyperentangled photon pairs using type-II spontaneous parametric down-conversion in a biperiod, 5% MgO-doped lithium-niobate ridge waveguide. The photon pairs are entangled in spatial mode and polarization degrees of freedom. A pulsed laser source at 687 nm, having an antisymmetric Hermite-Gaussian HG (1,0) spatial mode, is considered as the pump. Down-converted photon pairs, with the signal being at the telecommunication wavelength of 1550 nm, are characterized through a joint spectral amplitude analysis of their biphoton state.

DOI: 10.1103/PhysRevA.102.033722

I. INTRODUCTION

In the field of quantum technologies, quantum computation, quantum metrology, and quantum communication, entangled photon pairs play an important role [1]. When these photon pairs are entangled in more than one degree of freedom (DOF), they are said to be hyperentangled. Such hyperentangled photon pairs carry more information and are less sensitive against decoherence. Hence, they have potential applications in the field of quantum dense coding and quantum key distribution [2,3] and are excellent as long-distance information carriers [4]. In quantum communication, hyperentangled photon pairs can provide improved compatibility and long-distance communication through waveguides (WGs) and fibers.

Entangled photon pairs can be generated in a nonlinear optical medium through spontaneous parametric down-conversion (SPDC) which is the workhorse technique. SPDC in bulk crystals [5,6] and WGs is widely used to produce polarization-entangled photon pairs in either visible or telecom wavelengths [7–10]. In comparison to bulk crystals, nonlinear WGs are found to be an efficient way to generate such correlated photon pairs. Among many nonlinear optical materials, lithium niobate (LN) has emerged as a widely used medium, because of its transparency over a wide range of frequencies (0.35–0.45 μm) and high nonlinear coefficient. LN is also easily fabricated as waveguides. In comparison to other traditional WG structures, a ridge WG can confine light better and achieve higher conversion efficiency over a large bandwidth of operation with better power handling capabilities [11]. In particular, compared to rectangular WGs, they have low cutoff frequency, and low wave impedance [12–14]. Precise control on states of hyperentangled photons is very important for quantum communication. In this regard, the joint spectral amplitude (JSA) plays an important role in controlling the characteristics of the down-converted photons. The study of JSA deals with the structure and joint spectrum of the photons that aid to analyze the type of quantum correlation shared by the down-converted photon pairs [15]. In this paper, we have theoretically analyzed a unique case for postselection-free generation of photon pairs, hyperentangled in spatial mode and polarization DOFs, through type-II SPDC with an input, spatially antisymmetric pump beam incident on a biperiod LN WG. The signal photons are generated in the telecom wavelength. This study can be further extended to other types of WGs for generation of hyperentangled photon pairs in a wide spectral range.

II. STRUCTURAL DESIGN AND THEORETICAL ANALYSIS OF PDC IN A WAVEGUIDE

The dimensions of the ridge WG are $W = 6\,\mu$m, $D = 2.8\,\mu$m, and $h = 4.04\,\mu$m, as shown in Fig. 1. It is type-II quasi-phase-matched with two different cascaded poling periods, $\Lambda_1 = 6.561\,\mu$m and $\Lambda_2 = 7.2004\,\mu$m, simultaneously over a common length of $\mathcal{L} = 1$ cm. Here the nonlinear optical material [in yellow (light gray)] is a 5% MgO-doped LN and the cladding is made of SiO_2 [in blue (dark gray)]. The (red) dotted portion in Fig. 1(b) shows the WG core region.

We have used the relevant Sellmeier equations [16,17] for calculating the refractive indices of LN for different polarizations and wavelengths of light. In Fig. 2, we show the variation of the effective index as a function of wavelength for the fundamental TE and TM modes.

Using time-dependent perturbation theory, the photon joint state can be written as [18]

$$|\psi\rangle = BA_l^{(p)} \iint d\omega_s d\omega_i \sum_{\rho_\tau, M_\tau} \Big[A_{\rho_\tau, M_\tau}\, f_{\rho_\tau, M_\tau}(\omega_s, \omega_i) \times |\omega_s, \rho_s, M_s\rangle |\omega_i, \rho_i, M_i\rangle\Big], \quad (1)$$

where $\tau = (p, s, i)$ corresponds to pump, signal, and idler; ω_s and ω_i are the angular frequencies of signal and idler, respectively. ρ_τ ($\equiv H_\tau, V_\tau$) denotes the horizontal and vertical polarization indices, while, M_τ ($\equiv l, m, n$) denotes the spatial

*joyee@physics.iitd.ac.in

 ©2020 American Physical Society

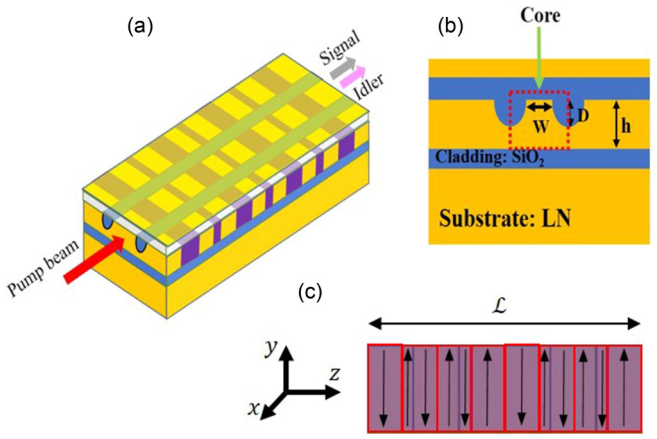

FIG. 1. (a) Schematic of the biperiod ridge waveguide having SiO_2 as cladding and 5% MgO-doped LN as core, achieved with cascaded poling periods $\Lambda_1 = 6.561\ \mu$m and $\Lambda_2 = 7.2004\ \mu$m. (b) Cross section of the waveguide. The waveguide dimensions are $h = 4.04\ \mu$m, $W = 6\ \mu$m, and $D = 2.8\ \mu$m, with length as $\mathcal{L} = 1$ cm. (c) Cascaded poling profile (side view).

mode indices of the pump, signal, and idler, respectively. B is an overall dimensionless constant [13]. $A_l^{(p)}$ is the overlap integral of the input beam field distribution $E_{\text{in}}^{\text{pump}}(\boldsymbol{r})$, at a frequency of ω_p, with the normalized field profile of the WG pump mode $u_{\rho_p,\,l}(\boldsymbol{r})$, defined as

$$A_l^{(p)} = \iint dr\, u^*_{\rho_p,l}\,(r) E_{\text{in}}^{\text{pump}}(r). \tag{2}$$

Now, in Eq. (1), $A_{\rho_\tau,\,M_\tau}$ represents the spatial overlap of the three interacting modes (pump, signal, and idler), defined as

$$A_{\rho_\tau,M_\tau} = \int_A dr u_{\rho_p,l}(r)\, u^*_{\rho_s,m}(r)\, u^*_{\rho_i,n}(r). \tag{3}$$

In Eq. (1), $f_{\rho_\tau,\,M_\tau}$ represents the joint spectral amplitude (JSA) of the two photons. The down-converted photon pairs

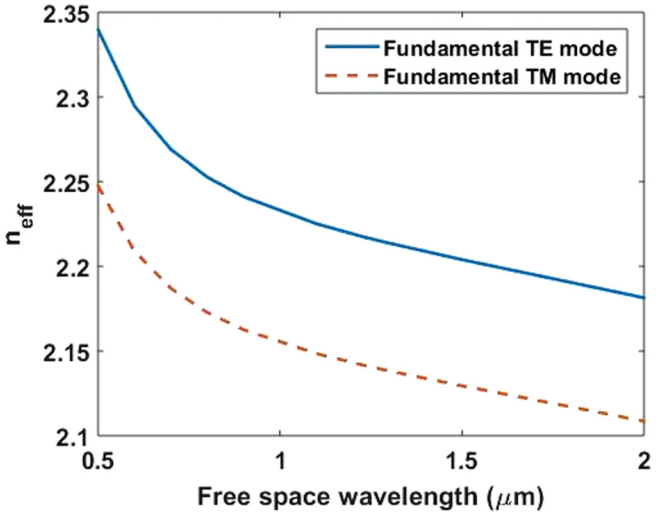

FIG. 2. Variation of the effective index of the waveguide with free-space wavelength for the fundamental TE mode (continuous curve), and TM mode (dashed curve).

in the SPDC process are correlated in frequency which can be described by their JSA. It depends on the properties of the incident pump beam and the nonlinear material used. Mathematically, JSA can be represented as the product of the pump envelope function (PEF) and the phase-matching function (PMF), as

$$f_{\rho_\tau,M_\tau}(\omega_s,\omega_i) = \alpha(\omega_s+\omega_i)\,\phi_{\rho_\tau,M_\tau}(\omega_s,\omega_i), \tag{4}$$

where $\alpha(\omega_s+\omega_i)$ is the PEF, defined as

$$\alpha(\omega_s+\omega_i) = e^{-\left(\frac{\omega_s+\omega_i-\omega_p}{\sigma_p}\right)^2}. \tag{5}$$

The PEF is considered to be a Gaussian function. Here σ_p is the bandwidth of the pulsed pump source about ω_p. The PMF is defined as

$$\phi_{\rho_\tau,M_\tau}(\omega_s,\omega_i) = \text{sinc}\left[\Delta\beta_{\rho_\tau,M_\tau}\frac{\mathcal{L}}{2}\right]\exp\left(i\Delta\beta_{\rho_\tau,M_\tau}\frac{\mathcal{L}}{2}\right), \tag{6}$$

where $\Delta\beta_{\rho_\tau,\,M_\tau}$ is the phase-matching condition in the WG having an additional quasi-phase-matching vector β_{QPM} to compensate the mismatch. The phase-matching conditions can be written as

$$\begin{aligned}&\Delta\beta_{\rho_\tau,M_\tau}(\omega_s,\omega_i)\\ &\quad= \beta_{\rho_p,l}\,(\omega_s+\omega_i) - \beta_{\rho_s,m}\,(\omega_s) - \beta_{\rho_i,n}\,(\omega_i) - \beta_{\text{QPM}},\end{aligned} \tag{7}$$

where $\beta_{\rho_\tau,M_\tau} = \frac{2\pi}{\lambda_\tau} n_{\rho_\tau,M_\tau}$, with n_{ρ_τ,M_τ} being the effective indices of different modes in the WG, and $\beta_{\text{QPM}} = \frac{2\pi}{\Lambda}$ is the quasi-phase-matching term corresponding to a poling period of Λ. Hence, from Eqs. (5) and (6) one can control the JSA by controlling the incident pump distribution and phase-matching function. If frequency is used as the identifier, the state in Eq. (1) can be represented as

$$\begin{aligned}|\psi\rangle = BA_l^{(p)}\iint d\omega_s d\omega_i \sum_{\rho_\tau,M_\tau}\big[&A_{\rho_\tau,M_\tau}\, f_{\rho_\tau,M_\tau}(\omega_s,\omega_i)\\ &\times|\rho_s,M_s\rangle_{\omega_s}|\rho_i,M_i\rangle_{\omega_i}\big].\end{aligned} \tag{8}$$

Similarly, mode number or polarization could also be used as identifiers for which Eq. (8) has to be represented accordingly.

III. GENERATION OF HYPERENTANGLED PHOTON PAIRS USING HERMITE GAUSSIAN HG (1,0) PUMP

In this study, we have considered a spatially antisymmetric Hermite-Gaussian HG (1,0) pump beam, for the generation of entangled photon pairs, whose input field is defined as

$$E_{\text{in}}^{\text{pump}}(\text{r}) = H_\mu\left(\frac{\sqrt{2}x}{a}\right)H_\nu\left(\frac{\sqrt{2}y}{b}\right)\exp\left[-\left(\frac{x^2}{a^2}+\frac{y^2}{b^2}\right)\right], \tag{9}$$

where H_ζ is a Hermite polynomial of order $\zeta = (\mu,\nu)$. Here (a,b) is the optimum (x,y) spot size of the pump beam. The launching position of the HG (1,0) pump beam in the WG is aligned in such a way that maximum energy gets coupled into the (1,0) pump mode of the WG, that is, $u_{\rho_p,l}$. The overlap integral in Eq. (2) with a maximum value of 0.97 corresponds to an optimized input beam with Gaussian X width $(2a) = 5\ \mu$m and Gaussian Y width $(2b) = 2.5\ \mu$m. We have computed

the signal and idler wavelengths and corresponding overlap integrals (A_{ρ_τ,M_τ}) for different SPDC mode conversions with the (1,0) pump mode of the WG, using biperiod poling periods $\Lambda_1 = 6.5612\,\mu$m and $\Lambda_2 = 7.2004\,\mu$m, corresponding to two different type-II phase-matching conditions, utilizing the nonlinear coefficient d_{24} in LN. This can be achieved through cascaded poling of the nonlinear medium [10,19], explained below. Thus, with a pump beam of wavelength $\lambda_p = 687$ nm and polarization $\rho_p = H_p$, for biperiod poling, Eqs. (3) and (7) can be elaborated as

$$\left(A_{\rho_\tau,M_\tau}\right)_{\Lambda_1} = \int_A dr\, u_{H_p,l}(r)\, u_{H_s,m}(r)\, u_{V_i,n}(r), \quad (10a)$$

$$\left(A_{\rho_\tau,M_\tau}\right)_{\Lambda_2} = \int_A dr\, u_{H_p,l}(r)\, u_{V_s,m}(r)\, u_{H_i,n}(r), \quad (10b)$$

and

$$\left(\Delta\beta_{\rho_\tau,M_\tau}\right)_{\Lambda_1} = \beta_{H_p,l}\,(\omega_s+\omega_i) - \beta_{H_s,m}\,(\omega_s) - \beta_{V_i,n}\,(\omega_i) - \frac{2\pi}{\Lambda_1}, \quad (11a)$$

$$\left(\Delta\beta_{\rho_\tau,M_\tau}\right)_{\Lambda_2} = \beta_{H_p,l}\,(\omega_s+\omega_i) - \beta_{V_s,m}\,(\omega_s) - \beta_{H_i,n}\,(\omega_i) - \frac{2\pi}{\Lambda_2}. \quad (11b)$$

Cascaded poling for satisfying simultaneous QPM conditions

The spatial variation of the relevant nonlinear coefficient along the direction of propagation provides the spatial frequencies. It is possible to simultaneously satisfy both QPM conditions if a periodic function with spatial frequency K_r is phase or amplitude modulated by another frequency K_s ($<K_r$) [10,19]. Then the modulated function would have spatial frequency components at $uK_r + vK_s$ with $u = \pm1, \pm2, \ldots$ and $v = \pm1, \pm2, \ldots$. The strength of the nonlinear interaction depends on the amplitude of the Fourier coefficients and, thus, only the lower-order terms are significant. Consider a domain reversal nonlinear medium with a period of $\Lambda_r = \frac{2\pi}{K_r}$ modulated by another domain reversal with a period of $\Lambda_s = \frac{2\pi}{K_s} (> \Lambda_r)$. Thus, the dependence of nonlinear coefficient d_{24} can be written as

$$\bar{d} = d_{24}\, g_1(z)\, g_2(z), \quad (12)$$

where

$$g_1(z) = +1, \quad 0 < z < \frac{\Lambda_r}{2},$$
$$= -1, \quad \frac{\Lambda_r}{2} < z < \Lambda_r,$$

with $g_1(z+\Lambda_r) = g_1(z)$.

Similarly,

$$g_2(z) = +1, \quad 0 < z < \frac{\Lambda_s}{2},$$
$$= -1, \quad \frac{\Lambda_s}{2} < z < \Lambda_s,$$

with $g_2(z+\Lambda_s) = g_2(z)$:

$$\bar{d} = \frac{4d_{24}}{\pi^2}(e^{iK_1 z} - e^{iK_2 z} + e^{-iK_1 z} - e^{iK_2 z}). \quad (13)$$

TABLE I. Computed values of the signal and idler wavelengths along with corresponding A_{ρ_τ,M_τ} values for different mode conversions with poling periods: $\Lambda_1 = 6.561\,\mu$m [for processes (i) and (ii)] and $\Lambda_2 = 7.2004\,\mu$m [for processes (iii) and (iv)], with $\lambda_p = 687$ nm.

$E_{H_p}(l_x, l_y) \rightarrow E_{H_s}(m_x, m_y) + E_{V_i}(n_x, n_y)$	λ_s (nm)	λ_i (nm)	$\lvert A_{\rho_\tau,M_\tau}\rvert$
(i) (1,0) → (0,0) + (1,0)	1550.0	1233.9	0.2082
(ii) (1,0) → (1,0) + (0,0)	1550.3	1233.7	0.2074
$E_{H_p}(l_x, l_y) \rightarrow E_{V_s}(m_x, m_y) + E_{H_i}(n_x, n_y)$	λ_s (nm)	λ_i (nm)	$\lvert A_{\rho_\tau,M_\tau}\rvert$
(iii) (1,0) → (0,0) + (1,0)	1550.0	1233.9	0.2091
(iv) (1,0) → (1,0) + (0,0)	1550.2	1233.8	0.2071

Assuming a square-wave variation with a 50% duty cycle, a simple Fourier series expansion of the function of $g_1(z)$ and $g_2(z)$ gives the frequencies $K_1 = K_r + K_s$ and $K_2 = K_r - K_s$. By choosing appropriate values of K_r and K_s, we can generate the required spatial frequencies to satisfy both QPM processes simultaneously. We have calculated the values of $K_r = 0.915$ and $K_s = 0.042$ considering the chosen values of $\Lambda_1 = 6.561\ \mu$m and $\Lambda_2 = 7.2004\,\mu$m, for the two QPM processes required in our case.

The parameters for these processes relevant to Eqs. (11a) and (11b) are given in Table I, that shows the relevant and most probable SPDC processes in the case of HG (1,0) input pump beam incident on the LN WG having the above two poling periods. Each poling period or phase-matching corresponds to two nearly equiprobable processes, such as processes (i) and (ii) that correspond to $\Lambda_1 = 6.561\ \mu$m.

In such a case, the phase-matching condition given by Eq. (11a) is satisfied by both these processes, and in particular, we can define $(\Delta\beta_{\rho_\tau,M_\tau})^{(\mathrm{i})}_{\Lambda_1}$ for process (i) with values of pump, signal, and idler mode numbers, $(l,m,n) \equiv (1,0,1)$, while $(\Delta\beta_{\rho_\tau,M_\tau})^{(\mathrm{ii})}_{\Lambda_1}$ for process (ii) with $(l,m,n) \equiv (1,1,0)$. Similarly, the phase-matching condition in Eq. (11b) is satisfied by both processes (iii) and (iv) that correspond to $\Lambda_2 = 7.2004\,\mu$m. Again, in particular, we can define $(\Delta\beta_{\rho_\tau,M_\tau})^{(\mathrm{iii})}_{\Lambda_2}$ and $(\Delta\beta_{\rho_\tau,M_\tau})^{(\mathrm{iv})}_{\Lambda_2}$ with $(l,m,n) \equiv (1,0,1)$ and $(1,1,0)$, respectively.

In these definitions, superscripts (i)–(iv) correspond to the respective processes in Table I. In all this, we have denoted "0" as the symmetric mode (0, 0), and "1" as the antisymmetric mode (1, 0) of the WG. Likewise, we can define $A^{(\mathrm{i})}_{\rho_\tau,M_\tau}$, $A^{(\mathrm{ii})}_{\rho_\tau,M_\tau}$, $A^{(\mathrm{iii})}_{\rho_\tau,M_\tau}$, and $A^{(\mathrm{iv})}_{\rho_\tau,M_\tau}$ as the overlap integrals of the pump, signal, and idler mode triplets for these four processes specific to the (l,m,n) values in each case. From Table I, another interesting feature is noted as follows. With a horizontally polarized, antisymmetric input HG (1,0) mode as the pump at $\lambda_p = 687$ nm, the signal photons are generated around 1550 nm while the idler photons are generated around 1233.9 nm. Hence these wavelengths (or frequencies ω_s and ω_i) could be the identifiers as depicted in Eq. (8). As we see, they are emitted in a combination of symmetric (0,0) and antisymmetric (1,0) modes of the WG with alternating possibilities among processes (i) and (ii) corresponding to Λ_1 and, similarly, processes (iii) and (iv) corresponding to Λ_2. In addition, they are also generated in a combination of horizontal and vertical polarizations with alternating possibilities among processes (i)

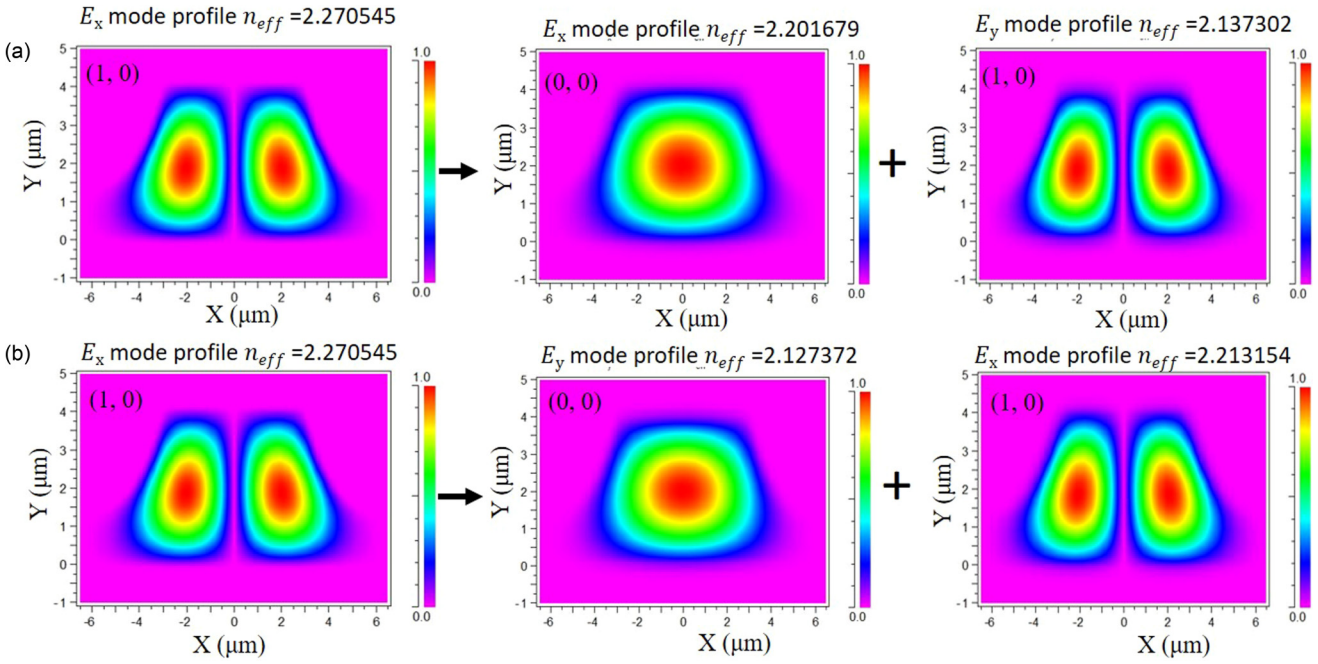

FIG. 3. (a) Mode conversions to different orders of the signal and idler spatial modes in type-II PDC process: (a) (1,0)→ (0,0) + (1,0) corresponding to process (i) in Table I, with $\Lambda_1 = 6.5612\ \mu$m, and (b) (1,0) → (0,0) + (1,0) corresponding to process (iii) in Table I, with $\Lambda_2 = 7.2004\ \mu$m.

and (iii) and, likewise, among (ii) and (iv). Figure 3 shows two of these PDC processes presented as (i) and (iii) in Table I with $\Lambda_1 = 6.5612\,\mu$m and $\Lambda_2 = 7.2004\,\mu$m, respectively. Thus, interestingly, such photon possesses correlations in multiple DOFs such as polarization, mode, and frequency and, hence, can be applied towards the study of hyperentangled photons. To see this clearly, consider the following. The PDC processes (i) and (ii) of Table I lead to a mode-entangled state as in Eq. (14a). Likewise, processes (iii) and (iv) lead to the state in Eq. (14b) [10]:

$$|\psi\rangle = \iint d\omega_s d\omega_i |H_s, V_i\rangle \otimes (C_1|0_s, 1_i\rangle + C_2|1_s, 0_i\rangle), \quad (14a)$$

$$|\psi\rangle = \iint d\omega_s d\omega_i |V_s, H_i\rangle \otimes (C_3|0_s, 1_i\rangle + C_4|1_s, 0_i\rangle). \quad (14b)$$

With $R = \frac{4d_{24}E_{H_{p,1}}\sqrt{\omega_s\omega_i}}{\pi^2}$, we define C_1, C_2, C_3, and C_4 as the probability amplitudes of the above four processes, respectively, as

$$C_1 = R\frac{A^{(i)}_{\rho_\tau,M_\tau}}{n_{H_s,0}n_{V_i,1}} e^{\frac{-i(\Delta\beta_{\rho_\tau,M_\tau})^{(i)}_{\Lambda_1}\mathcal{L}}{2}} \text{sinc}\left[\frac{(\Delta\beta_{\rho_\tau,M_\tau})^{(i)}_{\Lambda_1}\mathcal{L}}{2}\right], \quad (15a)$$

$$C_2 = R\frac{A^{(ii)}_{\rho_\tau,M_\tau}}{n_{H_s,1}n_{V_i,0}} e^{\frac{-i(\Delta\beta_{\rho_\tau,M_\tau})^{(ii)}_{\Lambda_1}\mathcal{L}}{2}} \text{sinc}\left[\frac{(\Delta\beta_{\rho_\tau,M_\tau})^{(ii)}_{\Lambda_1}\mathcal{L}}{2}\right], \quad (15b)$$

$$C_3 = R\frac{A^{(iii)}_{\rho_\tau,M_\tau}}{n_{V_s,0}n_{H_i,1}} e^{\frac{-i(\Delta\beta_{\rho_\tau,M_\tau})^{(iii)}_{\Lambda_2}\mathcal{L}}{2}} \text{sinc}\left[\frac{(\Delta\beta_{\rho_\tau,M_\tau})^{(iii)}_{\Lambda_2}\mathcal{L}}{2}\right], \quad (15c)$$

$$C_4 = R\frac{A^{(iv)}_{\rho_\tau,M_\tau}}{n_{V_s,1}n_{H_i,0}} e^{\frac{-i(\Delta\beta_{\rho_\tau,M_\tau})^{(iv)}_{\Lambda_2}\mathcal{L}}{2}} \text{sinc}\left[\frac{(\Delta\beta_{\rho_\tau,M_\tau})^{(iv)}_{\Lambda_2}\mathcal{L}}{2}\right]. \quad (15d)$$

The calculated signal bandwidths of the above four PDC processes (of Table I) are shown in Fig. 4. Sequentially, as shown in the legends, the processes are (i) $H_{p,1} \rightarrow H_{s,0} + V_{i,1}$ (red stars) with bandwidth ∼1.04 nm; (ii) $H_{p,1} \rightarrow H_{s,1} + V_{i,0}$ (black continuous) with bandwidth ∼1.17 nm; (iii) $H_{p,1} \rightarrow V_{s,0} + H_{i,1}$ (blue dotted) with bandwidth 0.79 nm; (iv) $H_{p,1} \rightarrow V_{s,1} + H_{i,0}$ (green triangles) with bandwidth ∼0.73 nm. We can predict a modal entanglement of the photons in an output collection bandwidth of 1549–1551 nm for the signal and 1233–1234.5 nm for the idler (not shown).

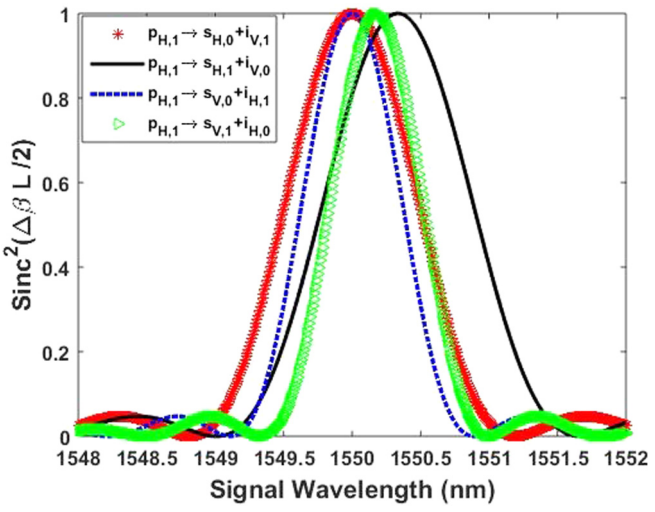

FIG. 4. Calculated signal bandwidths for PDC process $H_p \rightarrow H_s + V_i$ using $\Lambda_1 = 6.561\ \mu$m (red starred and black line) and PDC process $H_p \rightarrow V_s + H_i$ using $\Lambda_2 = 7.2004\ \mu$m (blue dotted and green triangles).

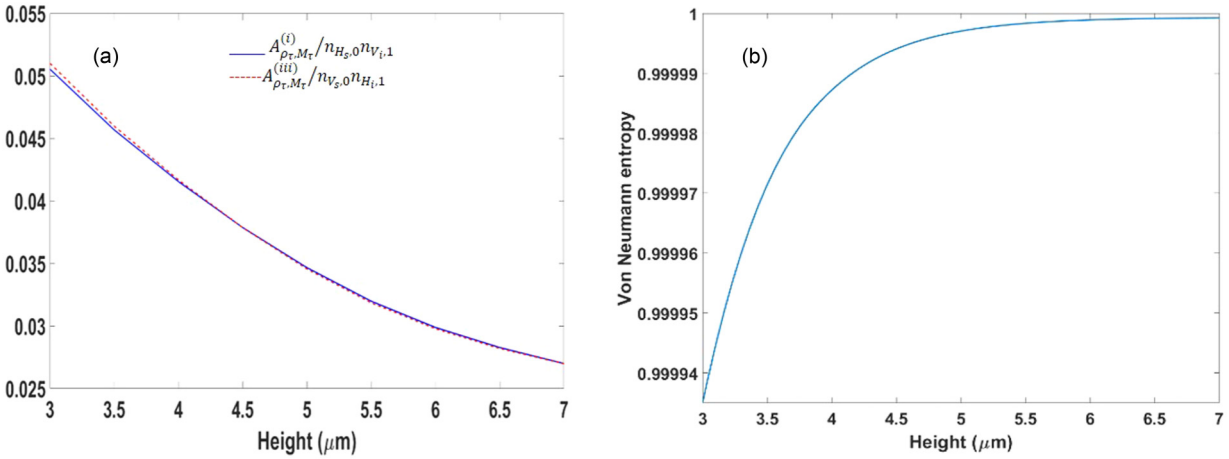

FIG. 5. Variation of (a) the effective overlap integrals: $A^{(i)}_{\rho_\tau,M_\tau}/n_{H_s,0}n_{V_i,1}$ and $A^{(iii)}_{\rho_\tau,M_\tau}/n_{V_s,0}n_{H_i,1}$, and (b) von Neumann entropy, with the height (h) of the waveguide, for a fixed width, $W = 6\ \mu$m.

All signal-idler pairs from these four, nearly equiprobable processes are generated together in the same WG. Note that the signal photons (around 1550 nm) and the idler photons (around 1233.9 nm) are modal entangled in the overlap region of their respective bandwidth curves: between *red starred and black* and between *blue dotted and green triangle curves.* Similarly, they are polarization entangled in the overlap between *red starred and blue dotted* and between *black and green triangle* curves. The photons are in a mixed state beyond these overlap regions. Within the common overlap bandwidth of all these four curves, in the central region, the generated photon pairs are in a hyperentangled state, both in polarization and spatial mode DOF, as stated in Eq. (16) below. This entangled state can be written by combining the states in Eqs. (14a) and (14b), and it is

$$|\psi\rangle = \iint d\omega_s d\omega_i (C_1|H_s 0_s, V_i 1_i\rangle + C_2|H_s 1_s, V_i 0_i\rangle) + (C_3|V_s 0_s, H_i 1_i\rangle + C_4|V_s 1_s, H_i 0_i\rangle). \quad (16)$$

Around perfect phase matching, $C_1 \approx C_2$ and $C_3 \approx C_4$, and Eq. (16) can be simplified as

$$|\psi\rangle = \iint d\omega_s d\omega_i (C_1|H_s, V_i\rangle + C_3|V_s, H_i\rangle) \otimes (|0_s, 1_i\rangle + |1_s, 0_i\rangle). \quad (17)$$

From Eq. (17), one can say that the joint state is hyperentangled in spatial mode as well as polarization. In order to achieve maximal entanglement in the above state, we can optimize the WG dimensions. Figure 5(a) shows a variation of the effective overlap integrals defined by Eqs. (10a) and (10b) as a function of the height of the WG, for a fixed width W and etching depth D. The corresponding von Neumann entropy for the state in Eq. (17) is calculated in Eq. (18) and plotted as a function of the height h of the WG, in Fig. 3(b). It is given as [10]

$$S = -\frac{|C_1|^2}{|C_1|^2 + |C_3|^2}\log_2\frac{|C_1|^2}{|C_1|^2 + |C_3|^2} - \frac{|C_3|^2}{|C_1|^2 + |C_3|^2}\log_2\frac{|C_3|^2}{|C_1|^2 + |C_3|^2}. \quad (18)$$

As we can infer, for our WG structure, a von Neumann entropy very close to unity, implying maximal entanglement, is achievable. Overall, Figs. 5(a) and 5(b) show that maximally entangled photon pairs, in the polarization as well as modal DOF, are achievable over a wide range of WG heights.

IV. JOINT SPECTRAL AMPLITUDE (JSA) ANALYSIS

In order to further characterize the frequency correlation properties of the photons, we also studied their joint spectral amplitude (JSA) that provides information about the different degrees of freedom of the photon pairs and their quantum correlations. We studied the JSA using Eq. (4), which is a product of PEF and PMF, expressed in Eqs. (5) and (6), respectively. The square modulus of these functions gives the corresponding intensities. Thus, in Fig. 6(a) we have plotted the pump envelope intensity (PEI) for the HG (1,0) mode of the WG whose width is directly proportional to the bandwidth of the pump beam, taken as $\sigma_p = 250$ GHz, and it is inclined at around 31° to the horizontal axis. As we know [14], PEI signifies the conservation of energy in the SPDC process. In Fig. 6(b), we have shown the phase-matching intensities (PMIs) for the four PDC processes (as in Table I), that arise from the conservation of momentum. The linewidth of the PMIs is inversely proportional to the length of the WG ($\mathcal{L} = 1$ cm). The yellow (bright) lines in the PMIs indicate $\Delta\beta_{\rho_\tau,M_\tau}(\omega_s, \omega_i) = 0$. The slope of the PMI curves, in Fig. 6(b) of these processes, is negative in each case, which indicates that the generated photons in different modes are negatively correlated in frequency. The slopes of the PMIs are different for the four processes shown due to a difference in group velocities at different frequencies. The PMIs are slightly curved which becomes visible if we plot them for longer wavelength ranges. This is due to dispersion in the WG, which is low in our case. When the radius of curvature of the PMIs is low it corresponds to a high dispersion, and vice versa. Note that an interesting feature in Fig. 6(b) is that the four PMI curves cross each other. This indicates that in the region of intersection, the phase-matching conditions are simultaneously satisfied for the four different PDC processes of Table I, in the same periodically poled lithium-niobate ridge waveguide with biperiod

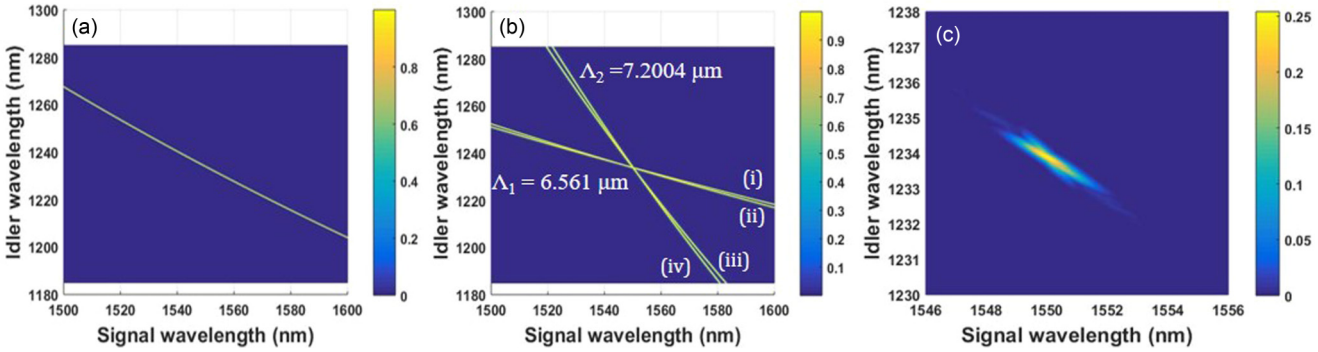

FIG. 6. (a) PEI of the pulsed pump with spatial HG (1,0) mode with bandwidth $\sigma_p = 250$ GHz, (b) PMIs of all four PDC processes, presented as (i)–(iv) of Table I, and (c) overlapped JSIs of these four processes.

poling at $\Lambda_1 = 6.561\ \mu$m and $\Lambda_2 = 7.2004\ \mu$m. Correspondingly, the overlapping JSIs of these four processes are shown in Fig 6(c). These JSI ellipses are negatively inclined again, indicating that the generated photon pairs in each process have a negative frequency correlation. Further, JSI analysis predicts that photons are hyperentangled in polarization and modal DOF approximately in an output collection bandwidth of 1549–1551 nm for the signal and 1233–1234.5 nm for the idler.

V. CONCLUSION

In conclusion, we have shown the possibility of generation of postselection-free, hyperentangled photons in a customized biperiod LN ridge WG incident with a spatially antisymmetric HG (1,0) pulsed pump beam. The modal analysis of the SPDC process was done by the finite element method (FEMSIM) to predict the optimal input parameters and to calculate the effective indices of the pump, signal, and idler modes for the WG, given the core-cladding index differences for the same. We find that with an antisymmetric HG (1,0) pump, due to parity conservation, the signal and idler photons can be generated in a combination of symmetric and antisymmetric spatial modes along with negative frequency correlation. Such photons possess correlations in multiple DOFs such as polarization, spatial mode, and frequency. Biperiod poling ensures that these photons are not only entangled in the spatial mode but also in the polarization DOF and can be collected in the output of the WG as hyperentangled photons without any postselection requirement. Moreover, a calculation of von Neumann entropy suggests that photons are entangled over a fairly wide range of the WG height. The JSI analysis further confirms the generation of these hyperentangled photon pairs.

Apart from entanglement, nondegenerate photons generated with a HG (1,0) pump beam mode can also be applied as a source of heralded single photons. Based on the detection of an idler photon generated in an antisymmetric mode of the WG corresponding to a particular wavelength, the partner signal photon can act like a single photon emitted in a symmetric mode, and in particular, in the fundamental (0,0) mode of the WG for certain cases. This is a further scope of our work.

An important aspect of the current study, which involves the JSA analysis, is that it describes the possibility of generation of hyperentangled photon pairs using a spatially antisymmetric input pump beam in a biperiod ridge WG scenario that has several advantages over other types of WGs.

ACKNOWLEDGMENTS

The authors thankfully acknowledge the following funding agencies: Department of Science & Technology, Ministry of Science and Technology, India (DST/ICPS/QuST/Theme-l/2019, Project No. 9), and Defence Research and Development Organisation (DFTM/03/3203/P/07/JATC-P2QP-07/463/D(R&D)). We appreciate initial discussions with Dr. Arun S. Patel on this work.

[1] O. Alibart, V. DAuria, M. De Micheli, F. Doutre, F. Kaiser, L. Labonte, T. Lunghi, E. Picholle, and S. Tanzilli, J. Opt. **18**, 104001 (2016).
[2] T.-C. Wei, J. T. Barreiro, and P. G. Kwiat, Phys. Rev. A **75**, 060305(R) (2007).
[3] X. F. Ren, G.-P. Guo, and G.-C. Guo, Phys. Lett. A **343**, 8 (2005).
[4] T. M. Graham, H. J. Bernstein, T.-C. Wei, M. Junge, and P. G. Kwiat, Nat. Commun. **6**, 7185 (2015).
[5] M. Fiorentino and R. G. Beausoleil, Opt. Express **16**, 20149 (2008).
[6] M. Hentschel, H. Hubel, A. Poppe, and A. Zeilinger, Opt. Express **17**, 23153 (2009).
[7] K. Banaszek, A. B. Uren, and I. A. Walmsley, Opt. Lett. **26**, 1367 (2001).
[8] S. Tanzilli, H. De Riedmatten, W. Tittel, H. Zbinden, P. Baldi, M. De Micheli, D. B. Ostrowsky, and N. Gisin, Electron. Lett. **37**, 26 (2001).
[9] M. Fiorentino, S. M. Spillane, R. G. Beausoleil, T. D. Roberts, P. Battle, and M. W. Munro, Opt. Express **15**, 7479 (2007).
[10] V. K. Shukla and J. Ghosh, Phys. Rev. A **101**, 023832 (2020).
[11] T. Umeki, O. Tadanaga, and M. Asobe, IEEE J. Quantum Electron. **46**, 1206 (2010).

[12] S. B. Cohn, Proc. IRE **35**, 783 (1947).
[13] S. Hopfer, IRE Trans. Microwave Theory Tech. **3**, 20 (1955).
[14] R. Kumar and J. Ghosh, J. Opt. **20**, 075202 (2018).
[15] R. B. Jin, R. Shimizu, K. Wakui, H. Benichi, and M. Sasaki, Opt. Express **21**, 10659 (2013).
[16] D. E. Zelmon, D. L. Small, and D. Jundt, J. Opt. Soc. Am. B **14**, 3319 (1997).
[17] O. Gayer, Z. Sacks, E. Galun, and A. Ariel, Appl. Phys. B **91**, 343 (2008).
[18] M. F. Saleh, B. E. A. Saleh, and M. C. Teich, Phys. Rev. A **79**, 053842 (2009).
[19] K. Thyagarajan, J. Lugani, S. Ghosh, K. Sinha, A. Martin, D. B. Ostrowsky, O. Alibart, and S. Tanzilli, Phys. Rev. A **80**, 052321 (2009).